

DNA Self-Assembly and Computation Studied with a Coarse-grained Dynamic Bonded Model

Carsten Svaneborg¹, Harold Fellermann^{1,2}, and Steen Rasmussen^{1,3}

¹ Center for Fundamental Living Technology, Department of Physics and Chemistry, University of Southern Denmark, Campusvej 55, DK-5320 Odense, Denmark

² ICREA-Complex Systems Lab, Universitat Pompeu Fabra (GRIB), Dr Aiguader 80, 08003 Barcelona, Spain

³ Santa Fe Institute, 1399 Hyde Park Road, Santa Fe NM 87501, USA
science@zqex.dk harold@sdu.dk steen@sdu.dk

Abstract We utilize a coarse-grained directional dynamic bonding DNA model [C. Svaneborg, Comp. Phys. Comm. (In Press DOI:10.1016/j.cpc.2012.03.005)] to study DNA self-assembly and DNA computation. In our DNA model, a single nucleotide is represented by a single interaction site, and complementary sites can hybridize reversibly. Along with the dynamic hybridization bonds, angular and dihedral bonds are dynamically introduced and removed to model the collective properties of double helix structure on the DNA zippering dynamics. We use this DNA model to simulate the temperature dependent self-assembly of DNA tetrahedra at several temperatures, a DNA icosahedron, and also strand displacement operations used in DNA computation.

1 Introduction

Ever since the pioneering work of Adleman in 1994 [1], DNA has been recognized as a massively parallel, versatile, and inexpensive computing substrate. In order for such substrate to be of practical interest, however, it is desirable that the computational framework is scalable and that individual computational elements, such as logical gates, can be combined to circuits of higher complexity. Recently, a scalable approach to enzyme-free DNA computing has been proposed where circuits consist of well mixed populations of relatively short DNA strands that communicate via strand displacement [17,14]. In this approach, individual gates consist of one DNA template that is composed of several logical domains. In their initial state, all domains but one are hybridized to one or more complementary strands and are therefore inert. The only exposed single strand domain of each gate is a short toehold region at one end of the template. This toehold region can reversibly bind a complementary signal strand which is designed to be longer than the toehold domain and complementary to the next domain(s) of the template. The newly binding signal is then able to hybridize to all matching domains of the template, thereby displacing strands that were previously bound [22]. The displaced strands are either fluorescently marked output signals, internal signals that can bind to toehold regions of downstream gates, or waste.

By choosing domains of appropriate length, it can be guaranteed that toehold binding is reversible, whereas the final strand displacement is effectively irreversible, thus computation is energetically downhill and kinetically irreversible, if and only if the correct input strands are present and match the logical setup of the gates. It has been shown that this approach leads to modular logic gates that enable the design of large scale DNA circuits [3,9].

Branched DNA molecular constructs has been utilized in the pioneering work of Seeman et al. to self-assemble into a variety of structures such as a cubes, a truncated octahedron as well as two and three dimensional lattices. [18,4,21,20] Numerous DNA self-assembled structures has been published in the literature, in the present paper we will study the self-assembly of DNA tetrahedra [6,5] build four DNA constructs with 3 branches and DNA icosahedra build out of twelve DNA constructs with 5 branches [2].

We are interested in studying the statistical mechanics of hybridizing DNA strands, and the resulting DNA self-assembly and DNA computation. With the present coarse-grained model, we intent to capture generic effects of reversible hybridization between complementary beads and chains build of such beads without investing computational power in atomistic details which are uninteresting for our present purpose. We have chosen a minimal DNA model that produces a simple ladder-like structure in the fully hybridized state because this model requires a minimum number of parameters to be specified. Single stranded DNA (ssDNA) is represented by a string of nucleotide beads connected by stiff springs representing directional backbone bonds. We also utilize angular interactions along the single strands to reproduce the persistence length of single stranded DNA. Instead of using a four letter alphabet representing the ACGT nucleotides, in the present paper we increase the alphabet maximally to avoid getting trapped in transient hybridized states. Physically, this corresponds to assuming that each bead represents a short sequence of nucleotides, and that two non-complementary beads or sequences are not able to hybridize with each other. We assume that the binding energy of all complementary beads are the same. We also assume that angular and dihedral interactions are independent of the types of beads involved.

A novel feature of our DNA model is that it involves dynamic hybridization bonds, which are introduced or removed between complementary interaction sites when they enter or exit the hybridization reaction radius. Along with the bonds, we dynamically introduce or remove angular and dihedral interactions in the chemical neighborhood of a hybridizing bead pair. These interactions are introduced based on the local bond and bead type pattern, and hence allows us to retain some effects of the local chemical structure in this coarse-grained model. We utilize bonds carrying directionality to represent the 3'-5' backbone structure of DNA molecules. This allows us to introduce dihedral interactions that can distinguish between parallel and anti-parallel strand alignments. We have implemented the dynamic bonding and directional bond framework – a modified version of the Large-scale Atomic/Molecular Massively Parallel Simulator [12,19] (LAMMPS).

The dynamic bonded DNA model combines the binary nature of the Poland-Scharaga (PS) model [13], the “one-site per nucleotide” coarse-grained model [16,15], and the sticky DNA interactions of nano-particle DNA models [10,11]. As in the PS model, dynamic bonded base pairs can either be hybridized or open. In the “one-site per nucleotide” coarse-grained DNA models [16,15], hybridized base pairs are represented by a continuous pair-potential, whereas in dynamic bonding DNA models, base pairs are characterized by a continuous bond potentials that can break. The dynamic bonding DNA models can also be regarded as being off-lattice generalizations of the real space lattice PS model [8], where a single DNA strand is described as a semi-flexible bead-spring polymer where complementary monomers will form hybridization bonds when they are close. The dynamic bonded DNA models are “one site per nucleotide” models, but we can also lump sequence of nucleotides into a single coarse-grained bead. In this case, we can, as a first approximation, assume that only beads representing complementary sequences can hybridize, and that the breaking of a hybridization bond corresponds to the creation of a DNA bubble. This would be a “many nucleotides per site” dynamic bonding DNA model more akin to the sticky site DNA models used to study model self-assembly of DNA functionalized nano-particles [7,10,11].

Sect. 2 presents the dynamic bonded DNA model, which we use to study self-assembly of DNA constructs and DNA-computing constructs in Sect. 3. We conclude with our conclusions in Sect. 4.

2 DNA model

The DNA model relies on two ingredients, a Langevin dynamic for propagating a system in time and space, and a dynamic directional bonding scheme [19] that propagates the chemical structure of the system. The force on bead i is given by a Langevin equation

$$\mathbf{F}_i = -\nabla_{\mathbf{R}_i} U - \frac{m}{\Gamma} \dot{\mathbf{R}}_i + \xi_i \quad \text{with} \quad U = U_{bond} + U_{angle} + U_{dihedral} + U_{pair}.$$

Here the first term denotes a conservative force derived from the potential U . The second term is a velocity dependent friction, and the third a stochastic driving force characterized by $\langle \xi_i^2(t) \rangle = k_B T m / (\Gamma \Delta t)$ and $\langle \xi_i(t) \xi_j(t') \rangle = \delta_{ij} \delta(t-t')$. The potential U depends on the positions of all the DNA beads and it comprises four terms representing bond, angular, dihedral, and non-bonded pair interactions, respectively. The friction and stochastic driving force implicitly represents the effect of a solvent with a specified friction and temperature. The Langevin dynamics is integrated using a Velocity Verlet algorithm with a time step $\Delta t = 0.001 \tau_L$ and $\Gamma = 2 \tau_L$ using a customized version of LAMMPS [12,19].

Here and in the rest of the paper we used reduced units defined by the Langevin dynamics and DNA model. The unit of energy is $\epsilon = k_B T$, where we chose to set Boltzmann’s constant k_B to unity, such that temperature is

measured in energy units. The unit of length σ is defined by the bead-to-bead distance along the backbone. This corresponds to the rise distance in a DNA double helix. The mass is $m = 1$ for all beads, this allows us to define a Langevin unit of time as $\tau_L = \sigma\sqrt{m/\epsilon}$. We can also use the diffusion relation $D_1(T) = \tau\sigma^2$ as an internal time unit τ . This represents the time it takes a single nucleotide bead to diffuse the rise distance of the double helix σ .

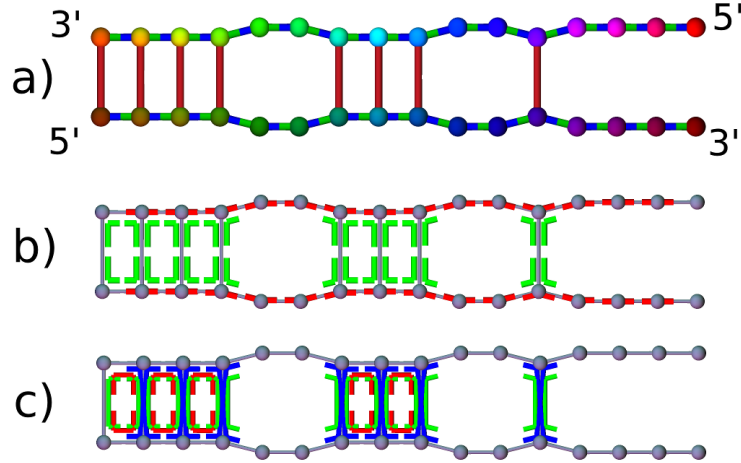


Figure 1. Illustration conformation of DNA model. a) complementary beads and hybridization bonds, b) angular interactions, c) dihedral interactions. The figure is explained in the text.

A single DNA molecule is build of nucleotide beads connected by bonds. Fig. 2a shows complementary nucleotide beads with the same hue but different levels of color saturation. As a simplification, we allow each bead only to hybridize with a single complementary bead. The DNA model has two types of bond interactions permanent backbone bonds and dynamic hybridization bonds. The hybridization bonds are shown as red lines, while permanent backbone bonds are shown green/blue lines, we explain why below. These two bonds are characterized by the two potential functions:

$$U_{bond,bb}(r) = \frac{U_{min,bb}}{(r_c^b - r_0^b)^2} ((r - r_0^b)^2 - (r_c^b - r_0^b)^2),$$

and

$$U_{bond,hyb}(r) = \begin{cases} \frac{U_{min,hyb}}{(r_c^h - r_0^h)^2} ((r - r_0^h)^2 - (r_c^h - r_0^h)^{-2}) & \text{for } r < r_c^h \\ 0 & \text{for } r \geq r_c^h \end{cases},$$

where the minimum of the potential is $U_{bond,bb}(r_0^b) = -U_{min,bb}$ and $U_{bond,bb}(r_c^b) = 0$ with $U_{min,bb} = 100\epsilon$, $r_0^b \equiv 1\sigma$, and $r_c^b = 1.2\sigma$. Dynamic hybridization bonds are characterized by $U_{bond,hyb}(r_0^h) = -U_{min,hyb}$ and $U_{bond,hyb}(r_c^h) = 0$ with $r_0^h = 2\sigma$ and $r_c^h = 2.2\sigma$. Note that $U_{bond,hyb}(r) \leq 0$ for all distances. The pair-interaction is given by a short-range soft-repulsive potential

$$U_{pair}(r) = A \left[1 + \cos \left(\frac{\pi r}{r_c^p} \right) \right] \quad \text{for } r < r_c^p,$$

where $A = 1\epsilon$ and $r_c^p = 1\sigma$. Angular and dihedral interactions are all characterized by the following potential function

$$U(\Theta; \Theta_0, U_{min}) = -\frac{U_{min}}{2} (\cos[\Theta - \Theta_0] + 1),$$

here $U(\Theta = \Theta_0; \Theta_0, U_{min}) = -U_{min}$, and $U(\Theta; \Theta_0, U_{min}) \leq 0$ for all angles Θ . In the DNA model we use a permanent angular interaction defined by $U(\Theta; \Theta_0 = \pi, U_{min} = 25\epsilon)$ along the backbone of single stranded DNA molecules to control the stiffness to a persistence length of $P \approx 12\sigma = 4nm$. In Fig. 2b backbone angular interactions are shown as thick red lines around the central bead defining the angle.

The dynamic directional bonding scheme, we have implemented, allows bonds to be dynamically introduced and removed during a simulation. When two non-hybridized beads of complementary type are within a reaction distance r_c^h a hybridization bond is introduced between them. If they e.g. through external forces or thermal fluctuations move further apart than r_c^h , the hybridization bond is broken. Fig. 2a shows an illustrative constructed DNA configuration where certain complementary beads are within the hybridization distance and have been hybridized, while the rest of the complementary beads are outside the hybridization distance and therefore remain non-bonded.

In real DNA molecules, the hydrogen bonds between Watson-Crick complementary nucleotides acts together with stacking interactions and the phosphodiester backbone bonds to give rise to a helical equilibrium structure of the double strand. In our coarse-grained model, the whole nucleotide is a single point-like particle, and we utilize angular and dihedral interactions to determine the equilibrium structure. To control the stiffness of the double stranded conformation and to ensure anti-parallel 3'-5' alignment of the two single strands, we have assigned directionality to the backbone bonds. [19] This is also necessitated by the fact that the 3' and 5' carbons of the sugar ring has been merged into the single nucleotide bead. Fig. 1a shows the backbond bonds using green in one end and blue in the other end which represents the 3' and 5' ends of the bond respectively. From the illustrative configuration we can also observe that two hybridized bonds are anti-parallel. In fact, the interactions prevent the parallel strand alignment from occurring.

When a hybridization bond is introduced, we also dynamically add angular interactions between the hybridization bond and the neighboring backbone bonds. These angular interactions are characterized by the potential $U(\Theta; \Theta_0 =$

$\pi/2, U_{min,a}$), which favors a right angle conformation. For a hybridization bond inside two strands, we introduce four such angles, and two for a hybridization bond at the end of a pair of strands. When a hybridization bond is broken, all the associated angular interactions are also removed. In Fig. 2b these angular interactions are shown as green lines indicating the angle.

Besides introducing angular interactions, we also dynamically introduce dihedral interactions. A dihedral interaction involves four beads connected by three bonds. The bonds can either be a hybridization bond H , a $3' - 5'$ backbone bond, or a $5' - 3'$ backbone bond. One dihedral interaction has the bond patterns $H \leftrightarrow (3' - 5') \leftrightarrow H$ or $H \leftrightarrow (5' - 3') \leftrightarrow H$, and controls the arrangement of two neighboring base-pairs. In Fig. 2c, this is illustrated by three red lines defining the three bonds on the dihedral. We characterize this dihedral interaction by $U(\Theta; \Theta_0 = 0, U_{min,d})$ which favors a planar (cis) conformation. Another dihedral interaction has the bond patterns $(3' - 5') \leftrightarrow H \leftrightarrow (3' - 5')$ or $(5' - 3') \leftrightarrow H \leftrightarrow (5' - 3')$, and controls the angle between the backbone bonds on opposite strands on either side of the hybridization bond. In Fig. 1c, this interaction is illustrated by three blue lines defining the three bonds in the dihedral. We characterized this interaction by $U(\Theta; \Theta_0 = \pi, U_{min,d}, a = 0)$ which favors parallel backbone (trans) conformation. The last dihedral interaction has the bond patterns $(3' - 5') \leftrightarrow H \leftrightarrow (5' - 3')$ or $(5' - 3') \leftrightarrow H \leftrightarrow (5' - 3')$, and controls the angle between the backbone bonds on the same side of a hybridization bond. In Fig. 1c, these are shown as three green lines defining the three bonds in the dihedral. We characterized this interaction by $U(\Theta; \Theta_0 = 0, U_{min,d})$ which favors a parallel (cis) conformation. Note that without the directional backbone bonds, we would not be able to distinguish between these two latter dihedrals, and the stiffness of the double strand would be entirely determined by the angular interactions of the single strands.

During a simulation, at each time we introduce a hybridization bond, we also introduce up to four angular interactions and up to eight dihedral interactions, less if the hybridization bond is at end of a strand. This can be observed by comparing the interactions for the illustrative configuration shown in Fig. 1. Each time a hybridization bond is broken, we remove all these interactions again, such that the angular and dihedral interactions are always consistent with the hybridization bonds that are present in the structure.

We define Δ as the total decrease in binding energy when two beads hybridize inside a chain, and we assign one third of this energy to bond, angular, and dihedral interactions, respectively. This choice does not affect the static properties of the model, which are entirely determined by the total energy associated with a conformation, however the choice does influence the dynamics of zipping and collective effects. Hence $U_{min,hyb} = \Delta/3$, $U_{min,a} = \Delta/12$, and $U_{min,d} = \Delta/18$. The last fraction is due to the fact that of the eight dihedral interactions created for a single hybridization bond, four of them is shared with a neighboring hybridization bond, and hence only contributes half of the the binding energy. In the present minimal DNA model, we use $\Delta = 10\epsilon$ as reference energy. This

essentially is a definition of the absolute melting temperature of the DNA model, since only the ratio Δ/T enters the partition function of the model.

The directional dynamic bonding framework is not limited to Langevin simulations nor the particular definition of DNA bead interactions above, hence the framework allows us to study and compare a large class of minimal DNA models, where we have just chosen one particular convenient model for the present paper. Since we do not invest computational power in simulating a solvent nor atoms, but only in the relative few coarse-grained DNA beads, the time spend per particle per step is approximately $1 \times 10^{-5}s$ on a standard PC.

3 Results

Three dimensional DNA structures can be build by utilizing the self-assembly properties of complementary strands and by linking several stands into a e.g. end-linked constructs. In particular, we have designed four constructs each comprising three end-linked 16 bead long strands. By designing the complementary of the strands, we have programmed the constructs to self-assemble into a tetrahedron[6,5]. We have also designed 12 DNA constructs each comprising 5 end-linked 8 bead long strands, these constructs self-assemble into an icosahedron[2]. We estimate that the melting temperatures are $T_m(8) \approx 1.3\epsilon$, and $T_m(16) \approx 1.6\epsilon$ from a separate set of melting simulations (not shown).

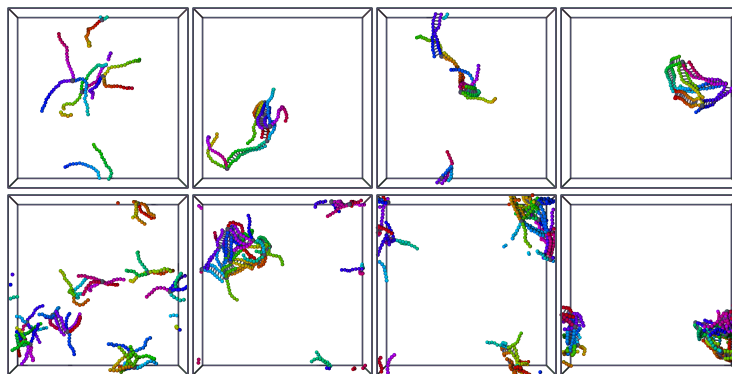


Figure 2. Self-assembly of tetrahedron from four 3-functional DNA constructs (top row) and icosahedron from twelve 5-functional DNA constructs (bottom row). Snapshots correspond to times $t = 1000\tau_L, 10.000\tau_L, 20.000\tau_L, 50.000\tau_L$ steps (top row), and for $t = 1000\tau_L, 20.000\tau_L, 30.000\tau_L, 50.000\tau_L$ steps (bottom row). Simulations have been performed at $T = 1.0\epsilon$. Complementary beads are shown with the same hue but different saturation. Note that periodic boundary conditions apply to the simulation box.

Fig. 2 shows visualizations of the DNA constructs during the self-assembly process. Initially the constructs are randomly placed into the simulation box.

Progressively, complementary strands hybridize with each other, and the constructs form fragments that ultimately yield the target structures. The time scale of the self-assembly dynamics is determined by the time it takes the constructs to diffuse, collide, and hybridize completely. Since we have the simulation trajectory, we can also characterize the detailed time dependence of the self-assembly dynamics. Fig. 3 shows the fraction of hybridized bonds as a function of time. By analyzing the bond structure, we can also count the number of structural fragments, that are not connected by bonds. For the icosahedron, we see a slow increase in the hybridized bond fraction towards unity as the structure is progressively assembled, while the number of fragments drops simultaneously from initially twelve free constructs to one when all constructs form a single icosahedron. The equilibrium hybridization bond fraction does not appear to be reached at the end of the simulation at $1 \times 10^8 \tau$. For the tetrahedra, we observe a similar increase in the fraction of hybridized bonds, however with six distinct steps corresponding to the edges of the tetrahedron.

The self-assembly dynamics is stochastic and depends on initial conditions and random diffusive motion. We have run some of the simulations twice to see how they approach equilibrium along different trajectories. The equilibrium hybridization bond fraction appears to have been reached by the tetrahedron self-assembly simulations. For tetrahedra, we observe that self-assembly at higher temperatures leads to a marked decrease in the average hybridization bond fraction similar to melting of DNA double strands. At $T = 1.8\epsilon$ the temperature is above the melting temperature of the DNA constructs, and they only transiently hybridize. Since we have a single fragment at equilibrium, the bond reduction is most likely due to DNA bubbles. From the data sets we can estimate that the melting temperature of the tetrahedron i.e. $\Theta(T_m) = 0.5$ is approximately $T_m(\text{Tetrahedron}) \approx 1.5\epsilon$.

Fig. 4 shows simulations of the strand displacement process underlying Seelig et al.'s DNA computing approach [17]. The top row shows the successful displacement of an initially hybridized 12 bead long signal strand from a 20 bead long template by a 20 bead long signal strand: once the signal strand diffuses to and binds to the toehold region, branch migration occurs quickly (during 300 time units) and the formerly bound signal strand is displaced irreversibly. The bottom row, on the other hand, shows how the displacement stalls in the presence of mismatches: here, a mismatch in the domain (last 10 beads) permits further hybridization of the signal strand. The newly binding and the original signal strand compete for matching bases in a random walk process until the non-matching strand dehybridizes again and leaves the gate available for potential matching signals (not present in the simulation).

Fig. 5 shows statistics of the displacement processes for several runs: the graphs depict hybridized bases of the original (red) and the newly binding signal strand (green), as well as the branch migration point (black). In the case of matching signals (top two simulations), it can be seen that displacement occurs quickly and essentially irreversible once the original strand is fully displaced. In the third simulation the signal strand and hybridized strand has the same

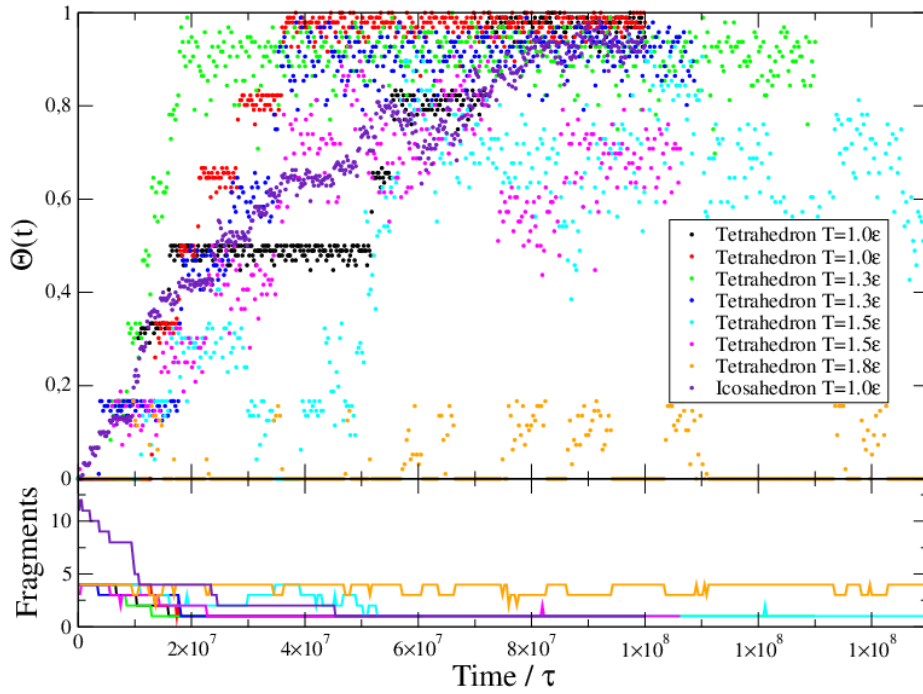


Figure 3. Fraction of hybridized bonds (top) and number of fragments (bottom) vs. time and temperature for self-assembly of tetrahedra and an icosahedron.

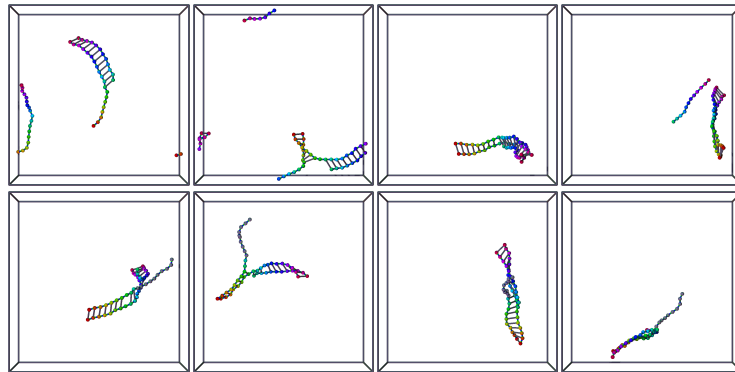


Figure 4. Simulations of strand displacement. A 20 bead long oligomer displaces a 12 bead long oligomer initially hybridized to a template for times $t = 500, 1,600, 1,700, 1,900\tau_L$ (top row). A 10 + 10 bead long oligomer where the latter half is non-complementary fails to displace a short oligomer hybridized to a template for times $t = 100, 3,000, 7,000, 10,000\tau_L$. Simulations are run at temperature $T = 1\epsilon$. Non-complementary beads are shown as gray.

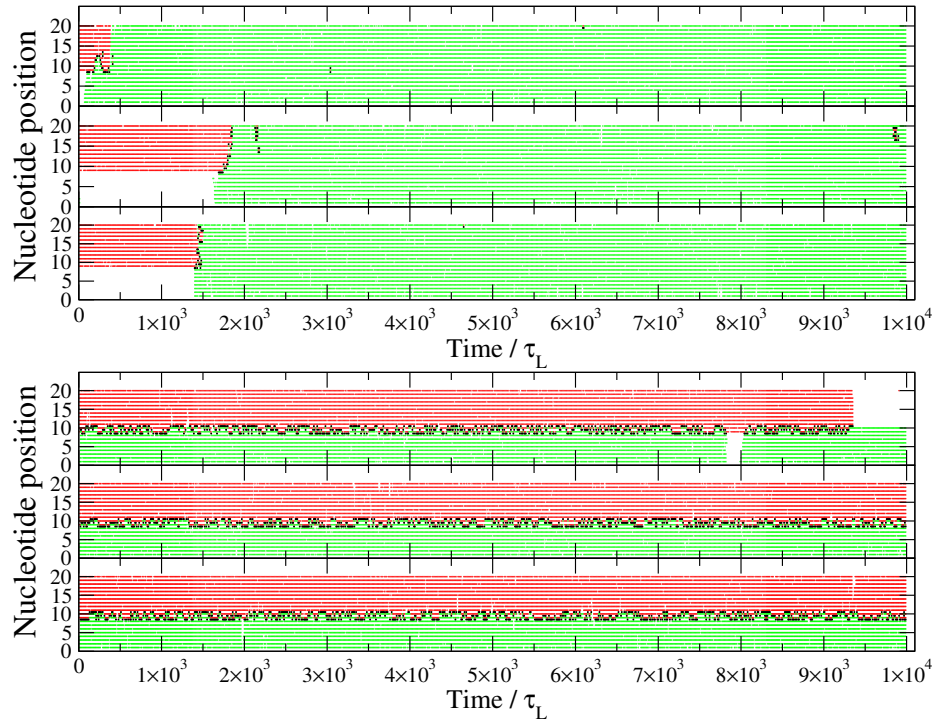


Figure 5. Time evolution of hybridization of oligomers on individual template nucleotides beads. The first simulation shows a 12 bead long complementary oligomer (red) being displaced by a 20 bead long complementary oligomer (green). The second simulation is identical to the first, but with different random initial conditions. The third simulation is of a 12 bead oligomer (red) competing with a 12 + 8 oligomer where the first half is complementary and the second half is non-complementary (green). The fourth simulation is of competition with a 10 + 10 oligomer. The fifth simulation is of competition with a 8 + 10 oligomer. The sixth simulation is of competition with a 5 + 10 oligomer. Also shown is the branch migration point (black).

length, and the interface is seen to diffuse forwards and backwards. A single dehybridization event is also observed for the original strand. In the case of mismatching signals (bottom three simulations), the displacement cannot proceed further than nucleotide 10, and the interface randomly moves between positions 8 and 10, until – occasionally – the mismatching signal dehybridizes from the toehold region (lack of green markers). In this case, the number of beads complementary to the toehold region (here 10, 8, and 5 beads) determines the equilibrium between hybridized and dehybridized configurations, and thus the performance and availability of the gate. Fig. 5 also depicts a source of potential failure in logical gates based on strand displacement, as the output signal can spontaneously dehybridize even in the absence of a matching input signal (as observed in the fourth simulation).

4 Conclusions

With these initial simulations, we have demonstrated that our coarse-grained DNA model can successfully simulate DNA assembly as well as DNA strand displacement dynamics which form the basis of state-of-the-art DNA computing approaches. We have successfully simulated self-assembly of DNA tetrahedra and icosahedra from four and twelve branched DNA constructs, respectively. Simulations show that the constructs self-assemble into the expected target structures.

We have further simulated successful displacement of an output strand when a matching input strand is present. In the presence of mismatches, we could demonstrate how the displacement process is prevented. Our simulations also capture potential failures of gates based on strand displacement, namely spontaneous release of the output strand in the absence of an input signal. These proof of concept simulations demonstrate how our coarse-grained model can be used to optimize the sequence, length and arrangement of toehold and domain structures in DNA computing approaches.

While such gate optimizations do not necessarily require spatially resolved models, our coarse-grained DNA model enables us to study systems that integrate DNA assembly and computing within a single framework. This enables us to use these simulations as a starting point for building and testing statistical mechanical theories describing these complex systems.

5 Acknowledgements

The research leading to these results has received funding from the European Community’s Seventh Framework Programme (FP7/2007-2013) under grant agreement n° 249032. Funding for this work is provided in part by the Danish National Research Foundation through the Center for Fundamental Living Technology (FLinT).

References

1. Adleman, L.M.: Molecular computation of solutions to combinatorial problem. *Science* 266(5187), 1021 (1994)
2. Bhatia, D., Mehtab, S., Krishnan, R., Indi, S.S., Basu, A., Krishnan, Y.: Icosahedral DNA nanocapsules by modular assembly. *Angew. Chem.* 121, 4198 (2009)
3. Cardelli, L.: Strand algebras for DNA computing. *Nat. Comput.* 10, 407 (2011)
4. Chen, J., Seeman, N.C.: Synthesis from DNA of a molecule with the connectivity of a cube. *Nature* 350, 631 (1991)
5. Erben, C.M., Goodman, R.P., J., T.A.: A self-assembled DNA bipyramid. *J. Am. Chem. Soc.* 129, 6992 (2007)
6. Goodman, R.P., Schaap, I.A.T., Tardin, C.F., Erben, C.M., Berry, R.M., Schmidt, C.F., Turberfield, A.J.: Rapid chiral assembly of rigid DNA building blocks for molecular nanofabrication. *Science* 310, 1661 (2005)
7. Hsu, C.W., Sciortino, F., Starr, F.W.: Theoretical description of a DNA-linked nanoparticle self-assembly. *Phys. Rev. Lett.* 105, 55502 (2010)
8. Jost, D., Everaers, R.: A unified description of poly- and oligonucleotide DNA melting: Nearest-neighbor, poland-scheraga and lattice models. *Phys. Rev. E* 75, 041918 (2007)
9. Lakin, M.R., Youssef, S., Cardelli, L., Phillips, A.: Abstractions for DNA circuit design. *J R Soc Interface* 9, 470 (2012)
10. Leunissen, M.E., Frenkel, D.: Numerical study of DNA-functionalised microparticles and nanoparticles: Explicit pair potentials and their implications for phase behavior. *J. Chem. Phys.* 134, 084702 (2011)
11. Martinez-Veracochea, F.J., Mladek, B.M., Tkachenko, A.V., Frenkel, D.: Design rule for colloidal crystals of DNA-functionalized particles. *Phys. Rev. Lett.* 107, 045902 (2011)
12. Plimpton, S.: Fast parallel algorithms for short-range molecular dynamics. *J. Comp. Phys.* 117, 1 (1995), <http://lammps.sandia.gov>
13. Poland, D., Scheraga, H.A.: Phase transitions in one dimension and the helix-coil transition in polyamino acids. *J. Chem. Phys.* 45, 1456 (1966)
14. Qian, L., Winfree, E.: Scaling up digital circuit computation with DNA strand displacement cascades. *Science* 332(6034), 1196 (2011)
15. Savelyev, A.: Do monovalent mobile ions affect DNA's flexibility at high salt content. *Phys. Chem. Chem. Phys.* 14, 2250 (2012)
16. Savelyev, A., Papoian, G.A.: Chemically accurate coarse graining of double-stranded DNA. *PNAS* 107, 20340 (2010)
17. Seelig, G., Soloveichik, D., Zhang, D.Y., Winfree, E.: Enzyme-free nucleic acid logic circuits. *Science* 314(5805), 1585 (2006)
18. Seeman, N.C.: Nucleic acid junctions and lattices. *J. Theor. Biol.* 99, 237 (1982)
19. Svaneborg, C.: LAMMPS Framework for Dynamic Bonding an Application Modeling DNA. *Comp. Phys. Comm.* In Press Doi: 10.1016/j.cpc.2012.03.005
20. Winfree, E., Liu, F., Wenzler, L.A., Seeman, N.C.: Design and self-assembly of two-dimensional DNA crystals. *Nature* 394, 529 (1998)
21. Xhang, Y., Seeman, N.C.: Construction of a DNA-truncated octahedron. *J. Am. Chem. Soc.* 116, 1661 (1994)
22. Zhang, D.Y., Winfree, E.: Control of DNA strand displacement kinetics using toe-hold exchange. *J. Am. Chem. Soc.* 131, 17303 (2009)